ACS OMEGA

http://pubs.acs.org/journal/acsodf

Article

Combination of Theoretical and Experimental Insights into the Oxygenated Fuel Poly(oxymethylene) Dibutyl Ether from *n*-Butanol and Paraformaldehyde

Gaojun An, Yangfeng Xia,* Zhenzhen Xue, Hongyan Shang, Sainan Cui, and Changbo Lu*

Cite This: *ACS Omega* 2022, 7, 3064−3072

Read Online

ACCESS | Metrics & More | Article Recommendations | Supporting Information

ABSTRACT: Oxygenated fuel has the function of self-supplying oxygen during the combustion process, which can greatly improve emission performance and reduce diesel fuel soot production. In this paper, a novel oxygenated fuel poly(oxymethylene) dibutyl ether ($PODBE_n$) is designed and synthesized through experiments in combination with density functional theory (DFT) calculation. The experimental results show that $PODBE_n$ has the advantages of high cetane number (73.6), moderate density (868 kg/m^3), and low condensation point (−72 °C). According to the DFT calculation results, the molecular ($PODBE_n$) polarity index of different polymerization degrees is similar to the value of diesel and has good mutual solubility with diesel. Moreover, the mechanism of the entire path of synthesis is calculated at the M06-2X/6-311G(d,p) level of theory. The energetic profile reveals that the rate-determining step is the nucleophilic addition step with the highest barrier energy (TS1 = 21.59 kcal/mol). This work provides a feasible method to synthesize high-performance oxygenated fuel $PODBE_n$ using NKC-9 ion-exchange resins.

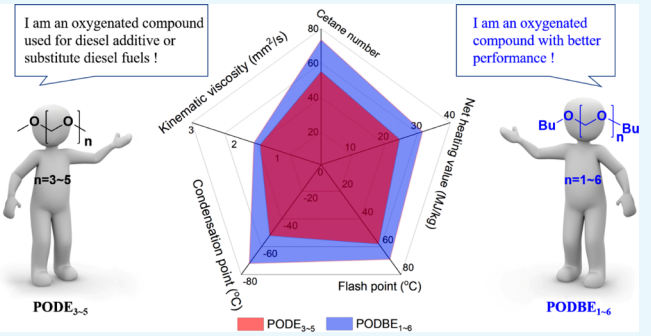

1. INTRODUCTION

It is well known that oxygenated fuels such as methanol, dimethyl ether (DME), and poly(oxymethylene) DME ($PODE_n$) can significantly reduce nitrogen oxides (NO_x) and particulate matter (PM) emissions when used as diesel fuel additives.[1−6] These oxygenated compounds have attracted much attention due to their clean energy properties. However, the physicochemical features of methanol and DME are considerably different from that of ordinary diesel fuels (such as high vapor pressure, low viscosity, and so on), requiring changes to the diesel engine infrastructure.[7−10] Compared with methanol or DME, $PODE_n$ has physicochemical properties similar to that of standard diesel. When used as a substitute for diesel fuel or a mixed fuel with diesel, it will not have a significant impact on the infrastructure of the diesel engine.[11,12] Furthermore, various pieces of literature have demonstrated that $PODE_n$ may effectively suppress NO_x and PM emissions due to its high oxygen content (45−50%).[13−17] As a result, $PODE_n$ is viewed as a viable oxygenated fuel for solving diesel pollution.

$PODE_n$ (molecular formula: $CH_3{-}O{-}(CH_2O)_n{-}CH_3$, where n is the degree of polymerization of the methoxy group) is a kind of polyether-oxidized fuel whose structure consists of a repeating unit $-(O{-}CH_2)_n-$ and two ending groups (methoxy ($-O{-}CH_3$) and methyl (CH_3)).[5,18−20] Among $PODE_n$ with different chain lengths (n = 1−8), medium-chain $PODE_{3-5}$ are considered to be more preferable for diesel additives due to their high oxygen content, moderate boiling range, and vapor pressure compared with diesel.[11,21−24] When the chain length of $PODE_n$ is short (n < 2), its flash point is too low to meet the safety standards, and when the chain length is long (n > 5), solid precipitation may form when mixed with conventional fuels and block the fuel system. Although $PODE_{3-5}$ have aroused widespread interest as diesel fuel additives, the industrial application of $PODE_n$ oxyfuel has not been carried out so far. The critical problem limiting $PODE_n$'s large-scale research and application is its high density (≥1.02 g/mL) and molecular polarity, which result in poor solubility with diesel at low temperatures.[25−27] Hence, it is very necessary and meaningful to develop a novel polyether-oxidized fuel with density and molecular polarity similar to that of diesel.

The manufacture of oxygen fuel poly(oxymethylene) dibutyl ether ($PODBE_n$, molecular formula: $C_4H_9{-}O{-}(CH_2O)_n{-}C_4H_9$, where n is the degree of polymerization of the methoxy group) from *n*-butanol and paraformaldehyde (PF) as reactants is described in this study. The main catalytic reaction

Received: November 16, 2021
Accepted: December 31, 2021
Published: January 11, 2022

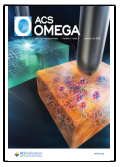

https://doi.org/10.1021/acsomega.1c06452
ACS Omega 2022, 7, 3064−3072

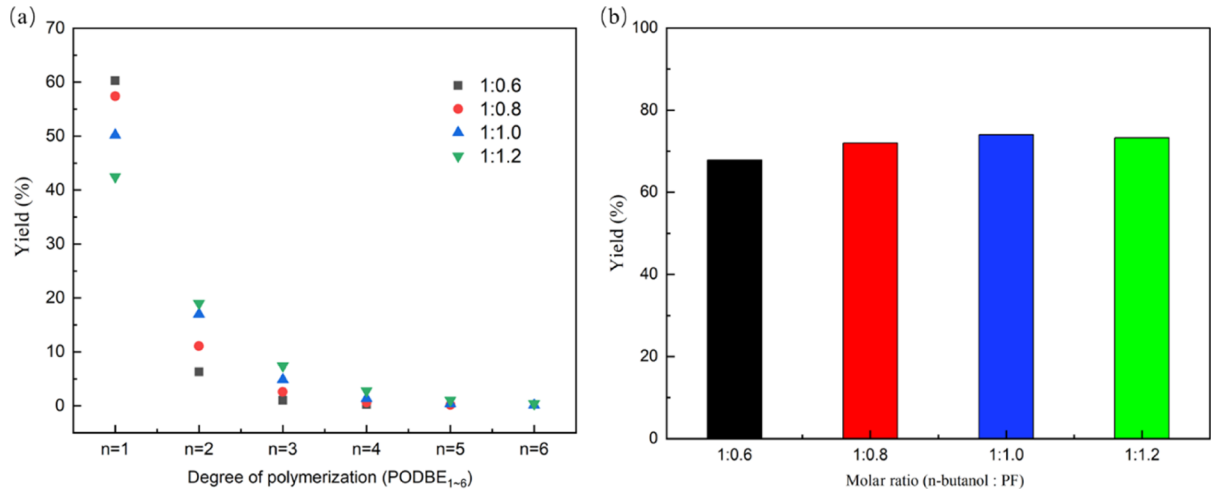

Figure 1. Influence of molar ratio (*n*-butanol/PF) on the distribution and yield of $PODBE_{1-6}$; (a) distribution of $PODBE_n$ (n = 1−6) and (b) yield of $PODBE_{1-6}$. Reaction conditions: NKC-9 (2 wt %); temperature, 100 °C; and time, 6 h.

parameters such as molar ratio, temperature, and reaction time have been evaluated in an autoclave reactor, with NKC-9 ion-exchange resin as a catalyst. In addition, the molecular polarity of $PODBE_n$ was examined using the molecular polarity index (MPI).[28,29] Electrostatic potential (ESP) was used to examine the charge distribution on the molecule surface.[30] The transition states (TSs) were calculated at the M06-2X/6-311G(d,p) level of theory. The weak interactions between different atoms were analyzed by noncovalent interactions (NCIs).[31]

2. RESULTS AND DISCUSSION

2.1. Synthesis of $PODBE_n$ (n = 1−6). *2.1.1. Influence of the Molar Ratio of n-Butanol and PF.* The molar ratio of the reactants is a key factor affecting the distribution and yield of different $PODBE_n$ polymers. The effect of n-butanol and PF molar ratios (1:0.6, 1:0.8, 1:1.0, 1:1.2, and 1:1.4) on the yield and product distribution of $PODBE_{1-6}$ was investigated using NKC-9 resin as a catalyst. Figure 1a shows that the distribution of the $PODBE_n$ (n = 1−4) polymer changes significantly as the molar ratio of *n*-butanol and PF increases. With the increase of PF molar ratio, the yield of $PODBE_1$ gradually decreased, while that of $PODBE_n$ (n = 2−4) gradually increased, indicating that the increase of PF molar ratio was beneficial to the formation of products with higher degree of polymerization. When the degree of polymerization "*n*" up to 5 or 6, the yield of $PODBE_n$ (n = 5∼6) was small (0.42%) and hardly changed with the PF molar ratio.

According to Figure 1b, as the PF molar ratio increases from 1:0.6 to 1:1.0, the overall yield of $PODBE_{1-6}$ steadily increases (from 68 to 74%). When the PF molar ratio is increased to 1:1.2, the overall yield of $PODBE_{1-6}$ nearly doubles (73%), indicating that the PF reaction concentration is saturated at this level. Therefore, further experiments were carried out under the condition that the molar ratio of *n*-butanol and PF was 1:1.0.

2.1.2. Influence of Reaction Temperature. Figure 2 illustrates the investigation of the effect of reaction temperature (from 70 to 110 °C) on the distribution and yield of $PODBE_{1-6}$. The yield of $PODBE_1$ gradually falls as the reaction temperature increases, but the yield of $PODBE_2$ rises and subsequently decreases, reaching a maximum value (17%)

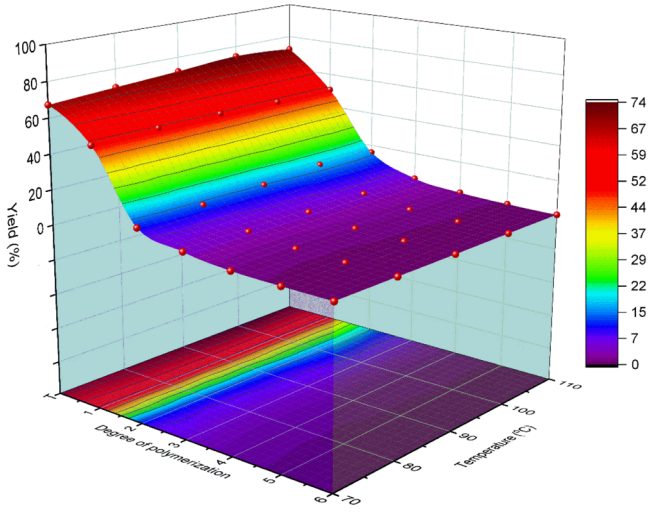

Figure 2. Influence of reaction temperature on the distribution and yield of $PODBE_{1-6}$; degree of polymerization T is the total yield of $PODBE_{1-6}$. Reaction conditions: NKC-9 (2 wt %); the molar ratio of *n*-butanol and PF was 1:1.0; time, 6 h.

at 100 °C, and the yield of $PODBE_{3-6}$ does not change considerably with the reaction temperature. With the temperature increase from 70 to 100 °C, the total yield of $PODBE_{1-6}$ increases from 67 to 74%. When the temperature rises to 110 °C, the overall yield of $PODBE_{1-6}$ falls to 72%. The internal structure of the reactor may be damaged as a result of the maximum reaction temperature of 110 °C of the NKC-9 resin collapsing, thereby reducing its catalytic efficiency. The results show that the appropriate temperature is 100 °C.

2.1.3. Influence of Reaction Time. The effect of reaction time (2, 4, 6, 8, and 10 h) on the yield and degree of polymerization of the product $PODBE_{1-6}$ was investigated (Figure 3). In terms of polymer distribution, as the reaction time grows, the yield of $PODBE_1$ decreases while the yield of $PODBE_{2-6}$ increases, showing that the degree of polymerization of the product increases with reaction time. As the time increases from 2 to 6 h, the yield of $PODBE_{1-6}$ increases from 68 to 74%. When the reaction time exceeds 6 h, the yield of $PODBE_{1-6}$ hardly changes, indicating that the reaction has

https://doi.org/10.1021/acsomega.1c06452
ACS Omega 2022, 7, 3064−3072

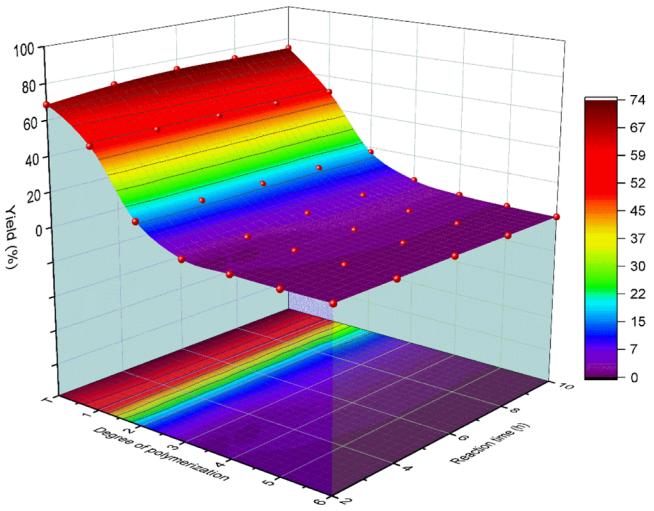

Figure 3. Influence of reaction time on the distribution and yield of $PODBE_{1-6}$; degree of polymerization T is the total yield of $PODBE_{1-6}$. Reaction conditions: NKC-9 (2 wt %); molar ratio of *n*-butanol and PF was 1:1.0; temperature, 100 °C.

reached equilibrium at this time. Hence, 6 h was chosen as the optimized reaction time.

2.2. Physical and Chemical Performance Analysis. To further assess $PODBE_n$'s effectiveness as a diesel-blending component, the physical and chemical properties of $PODBE_{1-6}$, $PODE_{3-5}$, and diesel were examined (Table 1).

Table 1. Physical and Chemical Properties of $PODBE_{1-6}$, $PODE_{3-5}$, and Diesel

entry	property	$PODBE_{1-6}$[a]	$PODE_{3-5}$[b]	diesel[c]
1	cetane number	73.6	55.2	50.9
2	net heating value (MJ/kg)	31.6	24.7	43.1
3	density 20 °C (kg/m^3)	868	1046	807
4	boiling range (°C)[d]	186−239	159−201	208−267
5	flash point (°C)	69	58	77
6	condensation point (°C)	−72	−52	−40
7	kinematic viscosity (mm^2/s)[e]	1.557	1.416	2.673

[a]$PODBE_1$ (67.9%), $PODBE_2$ (23.0%), $PODBE_3$ (6.5%), $PODBE_4$ (1.9%), $PODBE_5$ (0.57%), and $PODBE_6$ (0.18%). [b]$POBE_3$ (63.7%), $POBE_4$ (31.5%), and $POBE_5$ (3.7%). [c]−35# car diesel. [d]Distillation section (10 vol % to 90 vol %). [e]20 °C.

The cetane number is the most important metric for measuring the diesel combustion performance. Table 1 shows that the cetane number is listed in the following order: $PODBE_{1-6}$ (73.6) > $PODE_{3-5}$ (55.2) > diesel (50.9) (entry 1), indicating that $PODBE_{1-6}$ as a diesel-blending component can increase the diesel combustion performance significantly. Compared with the net heating value of $PODE_{3-5}$ (24.7 MJ/kg), $PODBE_{1-6}$ has a significant improvement (31.6 MJ/kg), which is beneficial to the fuel dynamic performance (entry 2). The density is listed in the order $PODE_{3-5}$ (1046 kg/m^3) > $PODBE_{1-6}$ (868 kg/m^3) > diesel (807 kg/m^3), showing that $PODBE_{1-6}$ is more compatible with diesel and is better suited as a diesel-blending component (entry 3). The condensation point of $PODBE_{1-6}$ (−72 °C) is much lower than that of diesel (−40 °C) and $PODE_{3-5}$ (−52 °C). This phenomenon shows that $PODBE_{1-6}$ has excellent low-temperature performance and can be applied in high-altitude and low-temperature areas (entry 6). In addition, $PODBE_{1-6}$ and $PODE_{3-5}$ have comparable boiling range and flash point values, matching the diesel requirement (entries 4 and 5).

Above all, $PODBE_n$ (n = 1−6) are more suitable than $PODE_n$ (n = 3−5) as diesel-blending components, and when mixed with diesel, they can significantly improve the combustion performance and low-temperature performance of diesel.

2.3. MPI Analysis. The ESP and MPI studies of the simulation oil (*n*-heptane + toluene + cyclohexane),[32] $PODE_{1-6}$, and $PODBE_{1-6}$ are shown in Figure 4 to compare the polarity of diesel, $PODE_{1-6}$, and $PODBE_{1-6}$ intuitively. The ESP distribution of *n*-heptane and cyclohexane in the simulation diesel is consistent (the molecular surface ESP distribution maps are entirely white), resulting in low molecular polarity (Figure 4a,b; MPI = 2.74 and 2.33 kcal/mol). The surface of the toluene molecule presents a negative ESP at the position of the benzene ring (the ESP distribution graph is blue), while the hydrogen atom presents a positive ESP (the ESP distribution graph is red), resulting in greater molecular polarity (Figure 4c; MPI = 7.90 kcal/mol).

ESP and MPI investigations of $PODE_{1-6}$ (Figure 4d−i) demonstrate that the oxygen atoms in the $PODE_{1-6}$ molecules display negative ESP, while the alkyl group exhibits positive ESP, resulting in an unequal distribution of the molecular surface. The MPI value shows an increasing trend as the degree of molecular polymerization increases, and the order follows: $PODE_1$ (13.55 kcal/mol) < $PODE_2$ (15.71 kcal/mol) < $PODE_3$ (17.12 kcal/mol) < $PODE_4$ (18.09 kcal/mol) < $PODE_5$ (18.82 kcal/mol) < $PODE_6$ (19.38 kcal/mol).

When compared to $PODE_{1-6}$, the MPI values of $PODBE_{1-6}$ are all lower, indicating that the value of $PODBE_{1-6}$ is closer to the molecular polarity of simulated diesel (Figure 4j−o). According to the rule of the likes dissolve each other, the compatibility of $PODBE_{1-6}$ with diesel is better than that of $PODE_{1-6}$ and is more suitable as a diesel-blending component.

2.4. Reaction Mechanism Analysis. *2.4.1. Entire Reaction Path.* Figure 5 shows a potential chemical pathway for the synthesis of $PODBE_n$ from n-butanol and PF. The reaction can be observed to be separated into two processes: (1) acetal reaction process; (2) chain growth process (Figure 5a). In the acetal reaction process, the condensation reaction between FA and *n*-butanol occurred to form the hemiacetal intermediate $BuOCH_2OH$. Due to its unstable nature, the intermediate hemiacetal readily interacts with *n*-butanol to generate $PODBE_1$. During the chain growth process, $PODBE_1$ was protonated by an acidic NKC-9 catalyst to generate the intermediate $BuOCH_2CHO^+Bu$, which then undergoes a nucleophilic substitution reaction with the monomer FA to yield $BuOCH_2OCH_2^+$ carbocations. Subsequently, the carbocation and *n*-butanol undergo a nucleophilic addition reaction to produce $BuOCH_2OCH_2^+$, which is further deprotonated to produce $PODBE_2$. Hence, $PODBE_3$, $PODBE_4$, $PODBE_5$, and $PODBE_6$ are similarly generated one by one.

2.4.2. Acetal Reaction Process Analysis. To deeply investigate the reaction mechanism, the reaction path of the acetal reaction process was first calculated by density functional theory (DFT) at the M06-2X/6-311G(d,p) level of theory, as shown in Figure 6. It can be seen from Figure 5b that the acetal reaction process consists of three main steps. The first step is a nucleophilic addition of FA to *n*-butanol, which results in the formation of the hemiacetal intermediate $BuOCH_2OH$. The TS1 connects reactant A and intermediate

https://doi.org/10.1021/acsomega.1c06452
ACS Omega 2022, 7, 3064−3072

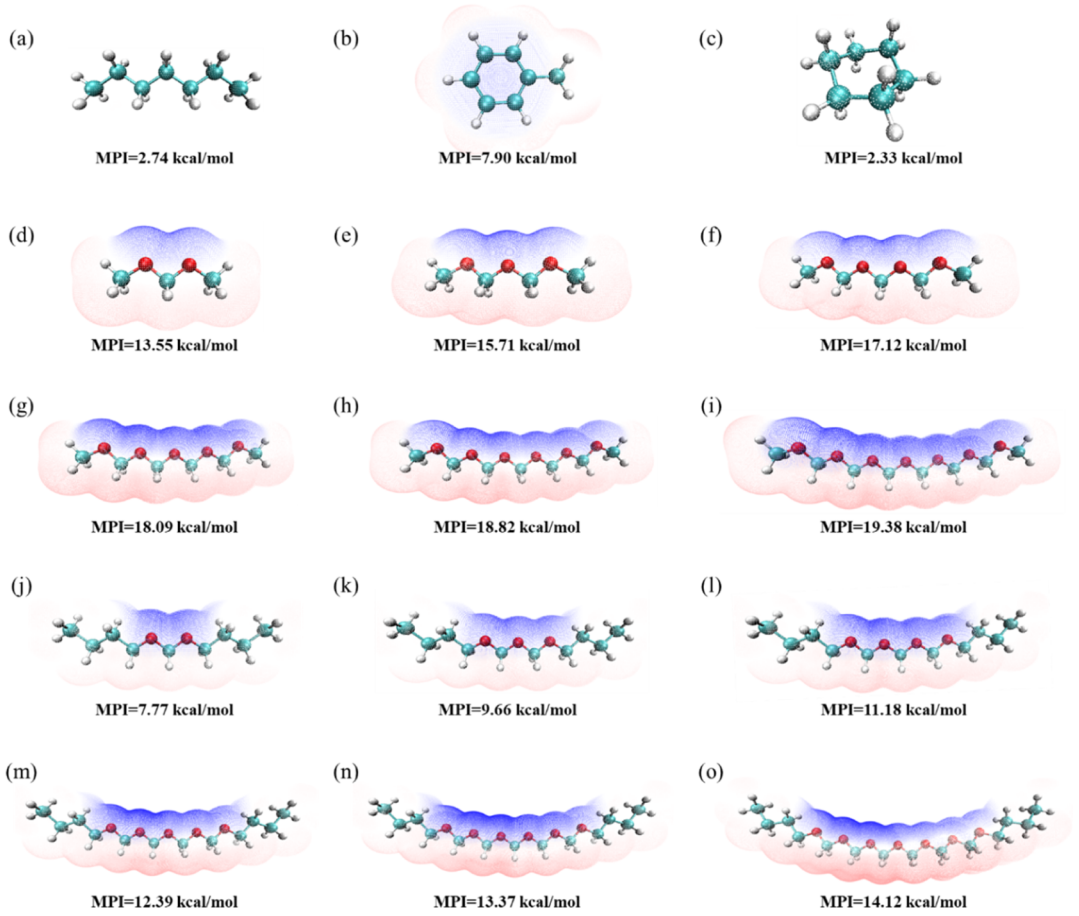

Figure 4. MPI analysis of diesel (model oil), $PODE_{1-6}$, and $PODBE_{1-6}$; (a) *n*-heptane; (b) toluene; (c) cyclohexane; (d) $PODE_1$; (e) $PODE_2$; (f) $PODE_3$; (g) $PODE_4$; (h) $PODE_5$; (i) $PODE_6$; (j) $PODBE_1$; (k) $PODBE_2$; (l) $PODBE_3$; (m) $PODBE_4$; (n) $PODBE_5$; and (o) $PODBE_6$.

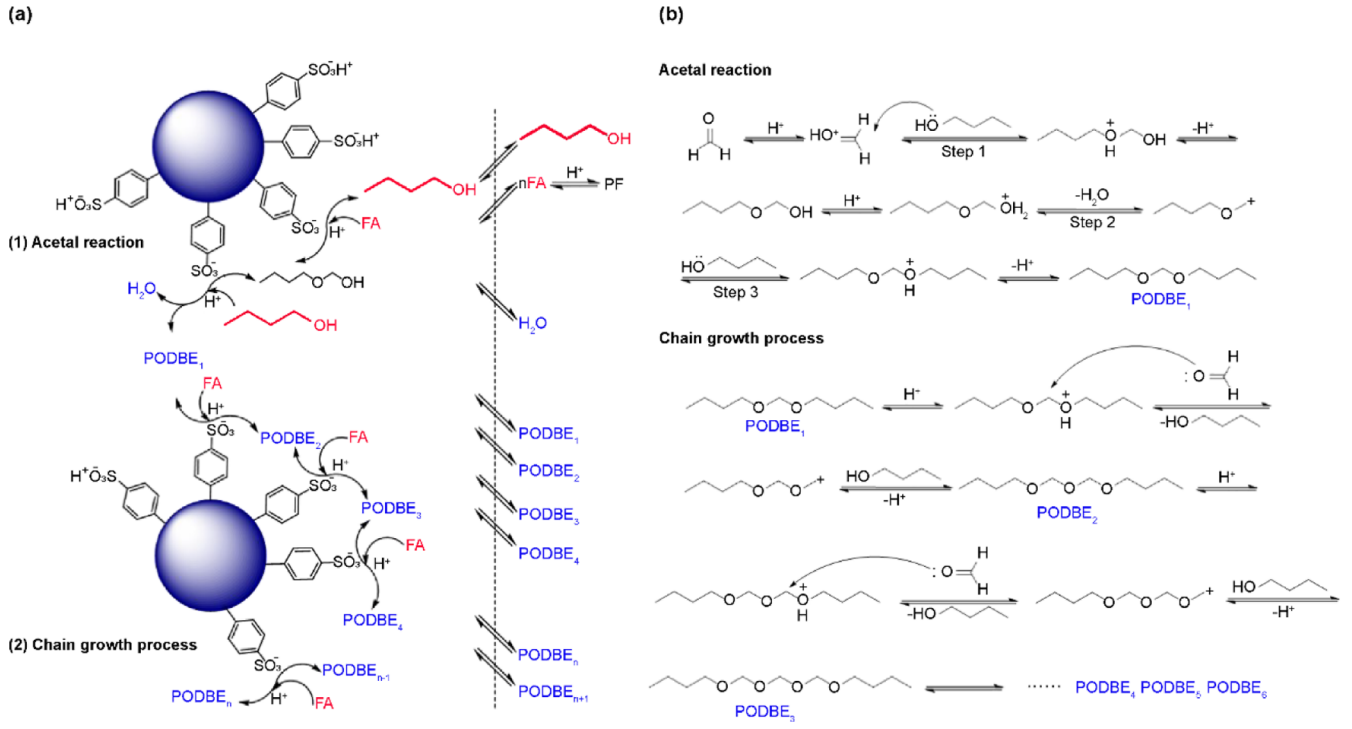

Figure 5. Possible reaction mechanism for the synthesis of $PODBE_{1-6}$ from PF and *n*-butanol; (a) reaction path and (b) mechanism detail.

https://doi.org/10.1021/acsomega.1c06452
ACS Omega 2022, 7, 3064−3072

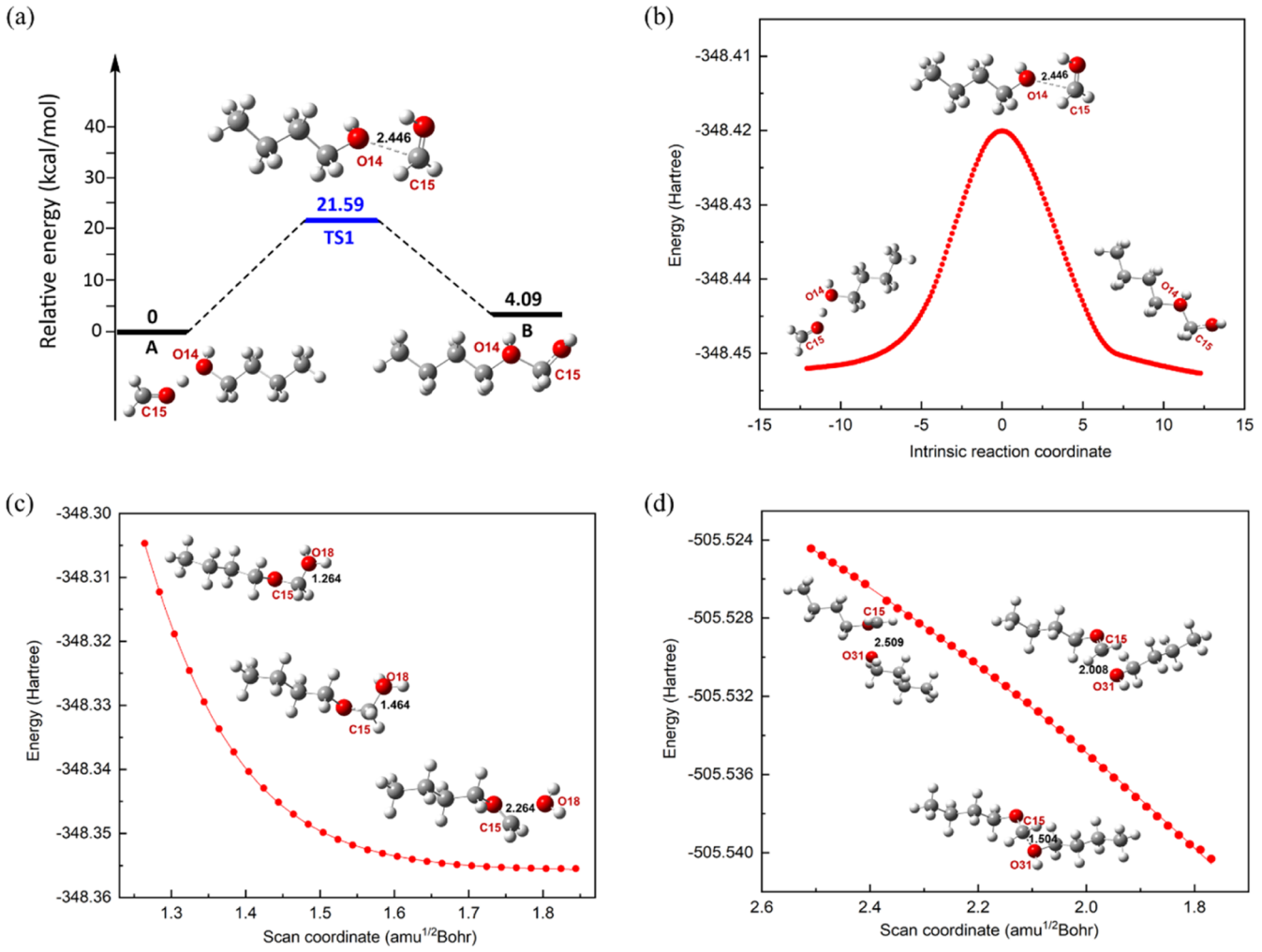

Figure 6. Energy studies of the acetal reaction process are as follows: (a) Gibbs free-energy barrier analysis, (b) IRC calculation, (c) energy analysis of the dehydration process, and (d) energy analysis of nucleophilic addition. The dashed lines represent the distances between two atoms in the structural development. The distance unit is Å.

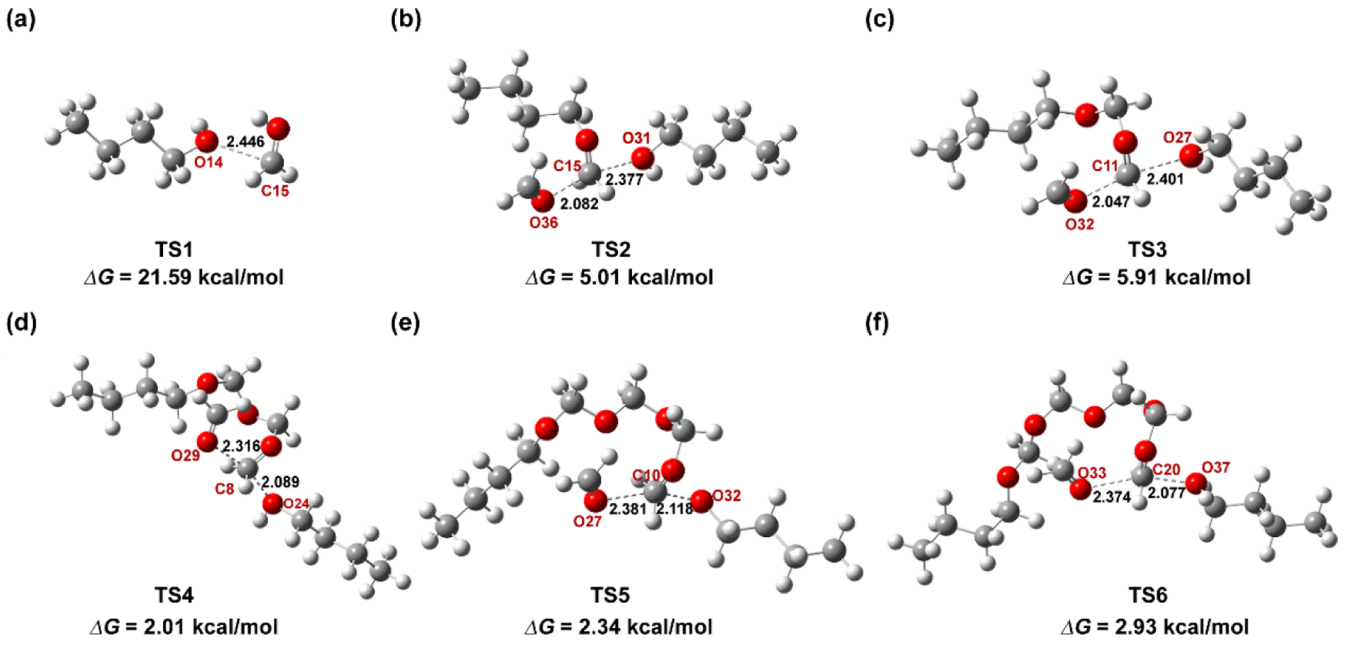

Figure 7. Optimized geometries of TS structures for the chain growth process: (a) TS1, (b) TS2, (c) TS3, (d) TS4, (e) TS5, and (f) TS6.

https://doi.org/10.1021/acsomega.1c06452
ACS Omega 2022, 7, 3064−3072

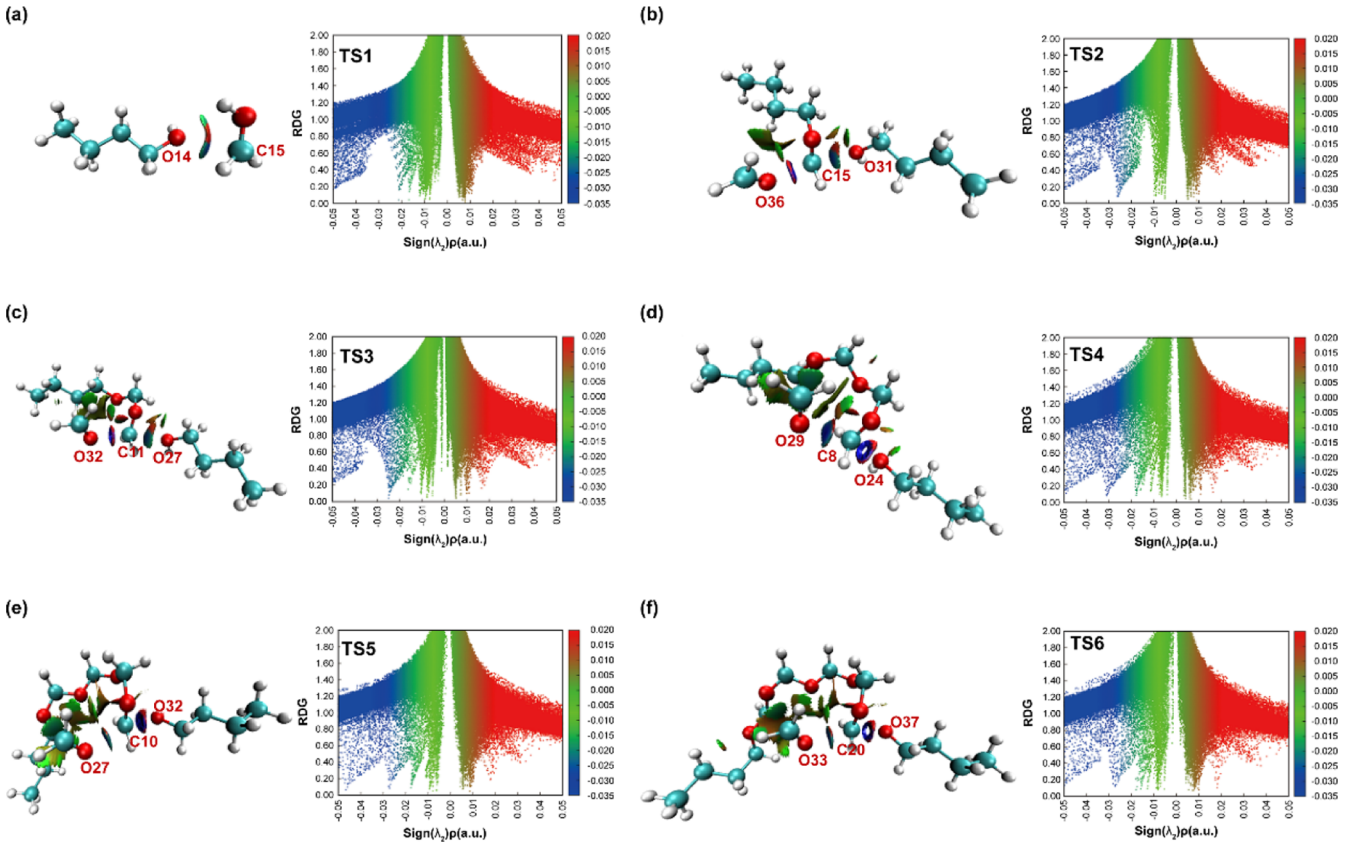

Figure 8. NCI plots for the optimized TS structures; (a) NCI analysis of TS1, (b) NCI analysis of TS2, (c) NCI analysis of TS3, (d) NCI analysis of TS4, (e) NCI analysis of TS5, and (f) NCI analysis of TS6. On the left are the equivalent 3D representations; the blue area indicates strong electrostatic interaction, while the green area reflects a more dispersive attractive interaction.

B with a free barrier energy of 21.59 kcal/mol in this step. Further, the O14 atom of n-butanol attacks the C15 atom of FA, resulting in the formation of a new chemical bond between O14 and C15 (Figure 6a). The intrinsic reaction coordinate (IRC) analysis of step 1 proved the correctness of the transition-state TS1 structure (Figure 6b). The second step includes a dehydration process and the formation of carbocation $BuOCH_2^+$. According to the energy scanning analysis, as the distance between O18 and C15 atoms rises (from 1.264 to 2.264), the total energy of the system decreases. This occurrence suggests that this stage is a spontaneous process with no TS structure (Figure 6c). The third step is the nucleophilic reaction between $BuOCH_2^+$ and *n*-butanol to form $BuOCH_2OH^+Bu$ and then across deprotonation to prepare $PODBE_1$. The energy scan analysis of this step shows that when the distance between C15 and O31 gradually closes (from 2.509 to 1.504 Å), the total energy of the system gradually decreases, indicating that this step is also a spontaneous process (Figure 6d).

2.4.3. Chain Growth Process Analysis. To further analyze the synthesis mechanism of $PODBE_{1-6}$, the main TS structures forming the target product $PODBE_n$ (n = 1−6) are listed in Figure 7. From Figure 5b, it is observed that the chain growth process mainly includes nucleophilic substitution reaction and nucleophilic reaction. As previously stated, the nucleophilic addition reaction between carbocation and *n*-butanol was a spontaneous reaction with no TS structures (Figure 6d). As a result, a complete TS analysis of the nucleophilic substitution process is critical for understanding the mechanism of $PODBE_n$ synthesis.

From Figure 7, it is observed that the value of free Gibbs barrier energy of TS1 (21.59 kcal/mol) is the highest among all TS structures. This investigation has demonstrated that the acetal reaction process's nucleophilic addition phase is the rate-determining step in the synthesis of $PODBE_{1-6}$. The free Gibbs barrier energies for TS2−TS6 are as follows: TS2 (5.01 kcal/mol) ≈ TS3 (5.01 kcal/mol) > TS4 (5.01 kcal/mol), TS5 (5.01 kcal/mol), and TS6 (5.01 kcal/mol). According to the reaction mechanism of the chain growth process, the products from $PODBE_1$ to $PODBE_6$ are sequentially generated in the order of the degree of polymerization n from small to large (Figure 5b), so the contents of $PODBE_{1-6}$ follow the sequence $n = 1 > n = 2 > n = 3 > n = 4 > n = 5 > n = 6$. Further, this sequence is consistent with the experimental results, verifying the reliability of the DFT calculation results.

Moreover, the TS structures are also analyzed by NCI, and the corresponding NCI maps are shown in Figure 8. In TS1 a blue circle isosurface is observed between O14 and C15, which means the O14 atom of *n*-butanol has a strong interaction with C15 of FA, thus resulting in the nucleophilic addition of *n*-butanol and FA (Figure 8a). The O atom of FA has a strong contact with the C atom of the carbocation in TS2−TS6, which facilitates the nucleophilic substitution process between FA and carbocation. The strong hydrogen bond between them is demonstrated by the blue circle isosurface distribution (Figure 8b−f).

3. CONCLUSIONS

In this research, a novel oxygen-containing fuel ($PODBE_{1-6}$) was formulated to overcome the limitations of PODE, such as

https://doi.org/10.1021/acsomega.1c06452
ACS Omega 2022, 7, 3064−3072

its high polarity, poor compatibility with diesel at low temperatures, and low heating value. The reaction parameters, physicochemical properties, and reaction mechanism of $PODBE_n$ were systematically investigated through experiments combined with DFT calculations. It was found that, under optimal conditions, the yield of $PODBE_{1-6}$ can reach 74%. The MPI tests of $PODE_{3-5}$, $PODBE_{1-6}$, and diesel (model oil) revealed that the polarity of $PODBE_n$ is closer to that of diesel than $PODE_n$, implying that it is theoretically more compatible with diesel. Furthermore, the physicochemical properties of $PODBE_{1-6}$ such as cetane number, heating value, density, and low-temperature performance have obvious advantages compared with that of $PODE_{3-5}$ and −35# diesel. DFT was used to calculate the mechanism of the complete path at the level of M06-2X/6-311G(d,p). The reaction consists of two processes, and the nucleophilic addition step with the highest Gibbs barrier energy (TS1 = 21.59 kcal/mol) is the rate-determining step.

4. EXPERIMENTAL SECTION

4.1. Materials. *n*-Butanol (99%), KBr (≥99.5%), and DMSO-d_6 (99.9%) were purchased from Aladdin Reagent (Shanghai, China). PF (≥96%) was purchased from Sinopharm Chemical Reagent (Beijing, China). NKC-9 acidic ion-exchange resin (H^+ type) was purchased from Tianjin Nankai Resin Technology Co., Ltd. (Tianjin, China). All reagents and chemicals were used directly without further purification and treatment.

4.2. Synthesis of $PODBE_n$. *n*-Butanol, PF, and NKC-9 (2 wt %) were added in a 0.5 L stirred autoclave reactor with a magnetic stirrer. The air within the reactor was changed three times with N_2 before the reaction began. The reaction conditions were optimized to be 1:0.6 to 1:1.2 *n*-butanol/HCHO mole ratio, 2−10 h reaction time, and 1.0 MPa reaction pressure. After the reaction, the autoclave was cooled to room temperature, the pressure in the autoclave was relieved, and then the reaction mixture was filtered to remove the catalyst NKC-9. To obtain pure products of $PODBE_1$, $PODBE_2$, and $PODBE_3$, the filtrate was deacidified with a deacidification agent and distilled at 90 mbar. Unfortunately, the reaction mixture contains inadequate $PODBE_4$, $PODBE_5$, and $PODBE_6$, and their boiling temperatures are too high. We cannot get pure $PODBE_4$, $PODBE_5$, and $PODBE_6$, so only their GC−MS characterization data are available.

4.2.1. $PODBE_1$. A colorless liquid. IR (KBr): ν = 2957, 2930, 2866, 1470, 1369, 1181, 1112, 1043, 1002, 933, 818, 736 cm^{-1}. ^1H NMR (600 MHz, d^6-DMSO): δ = 4.58 (s, 2H, CH_2), 3.45 (t, J = 6.5 Hz, 4H, CH_2), 1.49 (dd, J = 14.7, 6.7 Hz, 4H, CH_2), 1.34 (dd, J = 15.0, 7.4 Hz, 4H, CH_2), 0.89 ppm (t, J = 7.4 Hz, 6H, CH_3). ^{13}C NMR (151 MHz, d^6-DMSO): δ = 94.9 (O−C−O), 67.1 (C−O), 31.8 (CH_2), 19.4 (CH_2), 14.1 ppm (CH_3).

4.2.2. $PODBE_2$. A colorless liquid. IR (KBr): ν = 2962, 2935, 2862, 1456, 1383, 1195, 1108, 993, 938, 832, 736 cm^{-1}. ^1H NMR (600 MHz, d^6-DMSO): δ = 4.68 (s, 4H, CH_2), 3.48 (t, J = 6.6 Hz, 4H, CH_2), 1.49 (dt, J = 14.5, 6.6 Hz, 4H, CH_2), 1.33 (dd, J = 15.0, 7.5 Hz, 4H, CH_2), 0.88 ppm (t, J = 7.4 Hz, 6H, CH_3). ^{13}C NMR (151 MHz, d^6-DMSO): δ = 91.78 (O−C−O), 67.71(C−O), 31.72 (CH_2), 19.29 (CH_2), 14.09 ppm (CH_3).

4.2.3. $PODBE_3$. A colorless liquid. IR (KBr): ν = 2967, 2935, 2870, 1461, 1383, 1204, 1116, 970, 919, 823, 740 cm^{-1}. ^1H NMR (600 MHz, d^6-DMSO) δ = 4.77 (s, 2H, CH_2), 4.69 (s, 4H, CH_2), 3.48 (t, J = 6.6 Hz, 4H, CH_2), 1.53−1.43 (m, 4H, CH_2), 1.32 (dd, J = 15.0, 7.5 Hz, 4H, CH_2), 0.88 ppm (t, J = 7.4 Hz, 6H, CH_3). ^{13}C NMR (151 MHz, d^6-DMSO) δ = 92.21(O−C−O), 88.32 (O−C−O), 67.79 (C−O), 31.69 (CH_2), 19.27(CH_2), 14.08 ppm (CH_3).

4.3. Analysis Methods. The infrared (IR) spectra were obtained using an infrared spectrometer (Nicolet iS50, America), with KBr salt flakes serving as the test background. NMR spectra comprise ^1H NMR and ^{13}C NMR, which use a NMR spectrometer (Bruker AVANCE 600, Switzerland). The ^1H NMR working frequency is 600 MHz, the ^{13}C NMR working frequency is 151 MHz, and Me_4Si is used as an internal standard. The cetane number of oxygenated fuels is measured by a cetane number machine (Waukesha, America). The flash point of oxygenated fuels is measured by a flash point machine (PM-93, England). The condensation point test adopts a freezing point meter (DSA-70X, Canada) for measurement. The net heating value is measured by an automatic bomb calorimeter (6300, America). The density of the petroleum products tester is used to determine the density (DSY-412, China). The reactants and products are determined using a gas chromatograph (Agilent 7820A, America), with the selected HP-5 capillary column as the chromatographic column (30 m × 0.32 mm × 0.25 μm, America), and an FID detector. The column temperature programming conditions are as follows: initial temperature, 50 °C for 5 min; heating rate, 15 °C/min; and final temperature, 250 °C for 10 min. The detector temperature is 300 °C.

4.4. Calculated Details. All calculations were performed by Gaussian 09 software.[33] The geometries of $PODE_{1-6}$, $PODBE_{1-6}$, and diesel fuel surrogates were optimized at the M06-2X/6-311G(d,p) level of theory.[34] There are no negative eigenvalues in any of the optimized structures. A linear transit approach was used to search the TS structures, which revealed only one negative eigenvalue at no uncertain saddle point. Furthermore, IRC computations verified that all of the discovered TSs connected the reactants and products. The ESP analysis is based on the M06-2X/6-311G(d,p) level of theory. The ESP distribution on the surface of $PODBE_n$ molecules with different degrees of polymerization is also analyzed. The ESP map's blue−white−red colors represent the low, medium, and positive ESP levels in these regions, respectively. The polarity of different $PODBE_n$ molecules is quantitatively analyzed by comparing the values of different MPI (eq 1).[28]

$$\mathrm{MPI} = (1/A)\iint_S |V(r)|\mathrm{d}S \tag{1}$$

where A and $V(r)$ refer to the specific surface area and ESP value of point r in space, respectively, and dS refers to the integration of the molecular surface. The higher value of MPI indicates the strong molecular polarity of the compound.

■ ASSOCIATED CONTENT

Supporting Information

The Supporting Information is available free of charge at https://pubs.acs.org/doi/10.1021/acsomega.1c06452.

^1H NMR, ^{13}C NMR, and IR spectra of $PODBE_n$ and the Cartesian coordinates of optimized geometries of stable points calculated at the M06-2X/6-311G(d,p) level of theory (PDF)

https://doi.org/10.1021/acsomega.1c06452
ACS Omega 2022, 7, 3064−3072

AUTHOR INFORMATION

Corresponding Authors

Yangfeng Xia − *Beijing Institute of New Energy Technology, Beijing 102300, P. R. China;* orcid.org/0000-0003-1476-3845; Email: xiayangfeng17@mails.ucas.edu.cn

Changbo Lu − *Beijing Institute of New Energy Technology, Beijing 102300, P. R. China*; Email: luchangbo@vip.163.com

Authors

Gaojun An − *Beijing Institute of New Energy Technology, Beijing 102300, P. R. China*

Zhenzhen Xue − *Beijing Institute of New Energy Technology, Beijing 102300, P. R. China;* orcid.org/0000-0003-3603-6569

Hongyan Shang − *College of Science, China University of Petroleum, Qingdao, Shandong 266580, P. R. China*

Sainan Cui − *Beijing Institute of New Energy Technology, Beijing 102300, P. R. China*

Complete contact information is available at: https://pubs.acs.org/10.1021/acsomega.1c06452

Notes

The authors declare no competing financial interest.

ACKNOWLEDGMENTS

The authors would like to acknowledge the financial support from Beijing Institute of New Energy Technology.

REFERENCES

(1) Dong, X.; Jia, M.; Chang, Y.; Wang, P.; Niu, B. Kinetic modeling study of polycyclic aromatic hydrocarbon formation and oxidation for oxygenated fuels including methanol, n-butanol, methyl butanoate, and dimethyl ether. *Energy Fuels* **2020**, *34*, 4882−4898.

(2) Sezer, İ. Thermodynamic, performance and emission investigation of a diesel engine running on dimethyl ether and diethyl ether. *Int. J. Therm. Sci.* **2011**, *50*, 1594−1603.

(3) Tan, Y. R.; Botero, M. L.; Sheng, Y.; Dreyer, J. A. H.; Xu, R.; Yang, W.; Kraft, M. Sooting characteristics of polyoxymethylene dimethyl ether blends with diesel in a diffusion flame. *Fuel* **2018**, *224*, 499−506.

(4) Li, B.; Liu, H.; Wang, Z.; Wang, J. Combustion and emission characteristics of compression-ignition engines fuelled with oxygenated wide distillation fuel. *Qiche. Gongcheng./Automot. Eng.* **2017**, *39*, 1238−1244.

(5) Awad, O. I.; Ma, X.; Kamil, M.; Ali, O. M.; Ma, Y.; Shuai, S. Overview of polyoxymethylene dimethyl ether additive as an eco-friendly fuel for an internal combustion engine: Current application and environmental impacts. *Sci. Total Environ.* **2020**, *715*, 136849.

(6) Barrios, C. C.; Martín, C.; Domínguez-Sáez, A.; Álvarez, P.; Pujadas, M.; Casanova, J. Effects of the addition of oxygenated fuels as additives on combustion characteristics and particle number and size distribution emissions of a TDI diesel engine. *Fuel* **2014**, *132*, 93−100.

(7) Burger, J.; Ströfer, E.; Hasse, H. Chemical equilibrium and reaction kinetics of the heterogeneously catalyzed formation of poly(oxymethylene) dimethyl ethers from methylal and trioxane. *Ind. Eng. Chem. Res.* **2012**, *51*, 12751−12761.

(8) Ying, W.; Genbao, L.; Wei, Z.; Longbao, Z. Study on the application of DME/diesel blends in a diesel engine. *Fuel Process. Technol.* **2008**, *89*, 1272−1280.

(9) Zhao, X.; Ren, M.; Liu, Z. Critical solubility of dimethyl ether (DME)+diesel fuel and dimethyl carbonate (DMC)+diesel fuel. *Fuel* **2005**, *84*, 2380−2383.

(10) Park, W.; Park, S.; Reitz, R. D.; Kurtz, E. The effect of oxygenated fuel properties on diesel spray combustion and soot formation. *Combust. Flame* **2017**, *180*, 276−283.

(11) Burger, J.; Siegert, M.; Ströfer, E.; Hasse, H. Poly-(oxymethylene) dimethyl ethers as components of tailored diesel fuel: properties, synthesis and purification concepts. *Fuel* **2010**, *89*, 3315−3319.

(12) Lumpp, B.; Rothe, D.; Pastötter, C.; Lämmermann, R.; Jacob, E. Oxymethylene ethers as diesel fuel additives of the future. *MTZ Worldwide*, 2011; Vol. *72*, pp 34−38.

(13) Peláez, R.; Marín, P.; Ordóñez, S. Synthesis of poly-(oxymethylene) dimethyl ethers from methylal and trioxane over acidic ion exchange resins: a kinetic study. *Chem. Eng. J.* **2020**, *396*, 125305.

(14) Härtl, M.; Seidenspinner, P.; Jacob, E.; Wachtmeister, G. Oxygenate screening on a heavy-duty diesel engine and emission characteristics of highly oxygenated oxymethylene ether fuel OME_1. *Fuel* **2015**, *153*, 328−335.

(15) Qi, J.; Hu, Y.; Niu, J.; Ma, W.; Jiang, S.; Wang, Y.; Zhang, X.; Jiang, Y. Evaluation of polyoxymethylene dimethyl ethers as a new type of diesel additives. *Fuel* **2018**, *234*, 135−141.

(16) Song, H.; Kang, M.; Jin, F.; Wang, G.; Li, Z.; Chen, J. Brønsted-acidic ionic liquids as efficient catalysts for the synthesis of polyoxymethylene dialkyl ethers. *Chin. J. Catal.* **2017**, *38*, 853−861.

(17) Sun, R.; Delidovich, I.; Palkovits, R. Dimethoxymethane as a cleaner synthetic fuel: synthetic methods, catalysts, and reaction mechanism. *ACS Catal.* **2019**, *9*, 1298−1318.

(18) Zheng, Y.; Tang, Q.; Wang, T.; Wang, J. Kinetics of synthesis of polyoxymethylene dimethyl ethers from paraformaldehyde and dimethoxymethane catalyzed by ion-exchange resin. *Chem. Eng. Sci.* **2015**, *134*, 758−766.

(19) Li, H.; Song, H.; Chen, L.; Xia, C. Designed SO_4^{2-}/Fe_2O_3-SiO_2 solid acids for polyoxymethylene dimethyl ethers synthesis: The acid sites control and reaction pathways. *Appl. Catal., B* **2015**, *165*, 466−476.

(20) Lautenschütz, L.; Oestreich, D.; Seidenspinner, P.; Arnold, U.; Dinjus, E.; Sauer, J. Physico-chemical properties and fuel characteristics of oxymethylene dialkyl ethers. *Fuel* **2016**, *173*, 129−137.

(21) Zhang, X.; Oyedun, A. O.; Kumar, A.; Oestreich, D.; Arnold, U.; Sauer, J. An optimized process design for oxymethylene ether production from woody-biomass-derived syngas. *Biomass Bioenergy* **2016**, *90*, 7−14.

(22) Pellegrini, L.; Marchionna, M.; Patrini, R.; Beatrice, C.; Del Giacomo, N.; Guido, C. Combustion behaviour and emission performance of neat and blended polyoxymethylene dimethyl ethers in a light-duty diesel engine. *SAE Technical Paper*, 2012. 0148.7191.

(23) Pellegrini, L.; Marchionna, M.; Patrini, R.; Florio, S. Emission performance of neat and blended polyoxymethylene dimethyl ethers in an old light-duty diesel car. *SAE Technical Papers*, 2013; Vol. *2*.

(24) Zheng, Y.; Tang, Q.; Wang, T.; Liao, Y.; Wang, J. Synthesis of a green fuel additive over cation resins. *Chem. Eng. Technol.* **2013**, *36*, 1951−1956.

(25) Kang, M.-r.; Song, H.-y.; Jin, F.-x.; Chen, J. Synthesis and physicochemical characterization of polyoxymethylene dimethyl ethers. *J. Fuel Chem. Technol.* **2017**, *45*, 837−845.

(26) Song, H.; Liu, C.; Li, F.; Wang, Z.; He, X.; Shuai, S.; Wang, J. A comparative study of using diesel and $PODE_n$ as pilot fuels for natural gas dual-fuel combustion. *Fuel* **2017**, *188*, 418−426.

(27) Deng, X. D.; Han, D.; Li, X.; Li, D.; Sun, X.; Li, Y. Study on the effect of adding polyoxymethylene dimethyl ethers on properties of diesel fuel. *Contemp. Chem. Ind.* **2013**, *42*, 1508−1515.

(28) Liu, Z.; Lu, T.; Chen, Q. Intermolecular interaction characteristics of the all-carboatomic ring, cyclo [18] carbon: Focusing on molecular adsorption and stacking. *Carbon* **2021**, *171*, 514−523.

(29) Lu, T.; Chen, F. Multiwfn: A multifunctional wavefunction analyzer. *J. Comput. Chem.* **2012**, *33*, 580−592.

(30) Murray, J. S.; Politzer, P. The electrostatic potential: an overview. *Wiley Interdiscip. Rev.: Comput. Mol. Sci.* **2011**, *1*, 153−163.

(31) Xia, Y.; Zhang, Y.; Su, Q.; Dong, K. Theoretical insights into the effect of cations, anions, and water on fixation of CO_2 catalyzed by different ionic liquids. *ChemSusChem* **2020**, *13*, 6391−6400.
(32) Xiao, G.; Zhang, Y.; Lang, J. Kinetic modeling study of the ignition process of homogeneous charge compression ignition engine fueled with three-component diesel surrogate. *Ind. Eng. Chem. Res.* **2013**, *52*, 3732−3741.
(33) Frisch, M. J.; Trucks, G. W.; Schlegel, H. B.; Scuseria, G. E.; Robb, M. A.; Cheeseman, J. R.; Scalmani, G.; Barone, V.; Petersson, G. A.; Nakatsuji, H.; Li, X.; Caricato, M.; Marenich, A. V.; Bloino, J.; Janesko, B. G.; Gomperts, R.; Mennucci, B.; Hratchian, H. P.; Ortiz, J. V.; Izmaylov, A. F.; Sonnenberg, J. L.; Ding, F.; Lipparini, F.; Egidi, F.; Goings, J.; Peng, B.; Petrone, A.; Henderson, T.; Ranasinghe, D.; Zakrzewski, V. G.; Gao, J.; Rega, N.; Zheng, G.; Liang, W.; Hada, M.; Ehara, M.; Toyota, K.; Fukuda, R.; Hasegawa, J.; Ishida, M.; Nakajima, T.; Honda, Y.; Kitao, O.; Nakai, H.; Vreven, T.; Throssell, K.; Montgomery, J. A., Jr.; Peralta, J. E.; Ogliaro, F.; Bearpark, M. J.; Heyd, J. J.; Brothers, E. N.; Kudin, K. N.; Staroverov, V. N.; Keith, T. A.; Kobayashi, R.; Normand, J.; Raghavachari, K.; Rendell, A. P.; Burant, J. C.; Iyengar, S. S.; Tomasi, J.; Cossi, M.; Millam, J. M.; Klene, M.; Adamo, C.; Cammi, R.; Ochterski, J. W.; Martin, R. L.; Morokuma, K.; Farkas, O.; Foresman, J. B.; Fox, D. J. *Gaussian 09*, Rev. A.02; Gaussian, Inc.: Wallingford CT, 2009.
(34) Zhao, Y.; Truhlar, D. G. The M06 suite of density functionals for main group thermochemistry, thermochemical kinetics, noncovalent interactions, excited states, and transition elements: two new functionals and systematic testing of four M06-class functionals and 12 other functionals. *Theor. Chem. Acc.* **2008**, *119*, 525.

https://doi.org/10.1021/acsomega.1c06452
ACS Omega 2022, 7, 3064−3072